

# The Super-NFW model: an analytic dynamical model for cold dark matter haloes and elliptical galaxies

Edward J. Lilley,<sup>1</sup>★ N. Wyn Evans<sup>1</sup>, Jason L. Sanders<sup>1</sup>

<sup>1</sup>*Institute of Astronomy, Madingley Rd, Cambridge, CB3 0HA, UK*

Accepted XXX. Received YYY; in original form ZZZ

## ABSTRACT

An analytic galaxy model with  $\rho \sim r^{-1}$  at small radii and  $\rho \sim r^{-3.5}$  at large radii is presented. The asymptotic density fall-off is slower than the Hernquist model, but faster than the Navarro-Frenk-White (NFW) profile for dark matter haloes, and so in accord with recent evidence from cosmological simulations. The model provides the zeroth-order term in a biorthogonal basis function expansion, meaning that axisymmetric, triaxial and lopsided distortions can easily be added (much like the Hernquist model itself which is the zeroth-order term of the Hernquist-Ostriker expansion). The properties of the spherical model, including analytic distribution functions which are either isotropic, radially anisotropic or tangentially anisotropic, are discussed in some detail. The analogue of the mass-concentration relation for cosmological haloes is provided.

**Key words:** galaxies: haloes – galaxies: kinematics and dynamics – dark matter

## 1 INTRODUCTION

Analytic galaxy profiles provide simplicity for the modelling of galaxy components as well as insight into the dynamics of more realistic galaxies. For instance, the [Hernquist \(1990\)](#) galaxy model has the potential-density pair

$$\begin{aligned}\psi_{\text{H}} &= \frac{GM}{r+b}, \\ \rho_{\text{H}} &= \frac{Mb}{2\pi} \frac{1}{r(r+b)^3},\end{aligned}\quad (1)$$

where  $b$  is a parameter with the dimensions of length. It is related to the effective radius (or the radius of contour of surface density enclosing half the mass) by  $R_e = 1.815b$ . This profile is often used to model dark haloes which are believed to have the universal or [Navarro, Frenk & White \(1997\)](#), henceforth NFW) form

$$\begin{aligned}\psi_{\text{NFW}} &= \frac{4\pi G\rho_0 r_s^3}{r} \log(r+r_s), \\ \rho_{\text{NFW}} &= \frac{\rho_0 r_s^3}{r(r+r_s)^2},\end{aligned}\quad (2)$$

where  $r_s$  is a scalelength related to the virial radius. The asymptotic fall-off of the density in the Hernquist model is  $\rho_{\text{H}} \sim r^{-4}$ , so it avoids the defect of infinite mass which afflicts the NFW halo with  $\rho_{\text{NFW}} \sim r^{-3}$ . Additionally, the Hernquist model is often used to represent bulges and elliptical galaxies as it follows the [de Vaucouleurs \(1953\)](#) profile to a good approximation.

In this paper, we introduce the *super-NFW (or sNFW) model*, which has density and potential pair:

$$\begin{aligned}\psi_{\text{sNFW}} &= \frac{GM}{r+a+\sqrt{a}\sqrt{r+a}} \\ \rho_{\text{sNFW}} &= \frac{3M\sqrt{a}}{16\pi} \frac{1}{r(r+a)^{5/2}},\end{aligned}\quad (3)$$

where  $a$  is related to the effective radius by  $R_e = 5.478a$ .

Why is it ‘super-NFW’? The model provide a good match to cosmological haloes, but it has finite mass as the density falls off more slowly like  $\rho_{\text{sNFW}} \sim r^{-3.5}$ . This is slower than the Hernquist model, but faster than the NFW. Recent work on the splashback radius ([Diemer et al. 2017](#)) suggests that the density of cosmological haloes drops more rapidly than NFW, but slower than Hernquist, at large radii. There are of course other models in the literature that have  $\rho \propto r^{-1}$  at the centre and have an asymptotic fall off with logarithmic gradient between  $-3$  and  $-4$  (e.g. [An & Evans 2006](#); [An & Zhao 2013](#)). The super-NFW model however has another special property – it is the zeroth-order term of a biorthogonal expansion ([Lilley et al. 2017](#), henceforth Paper II). The potential-density pairs of arbitrarily distorted sNFW models are, therefore, straightforward to construct. This is important as cosmological dark haloes show many deviations from spherical symmetry, and therefore a spherical model is only good to crudest order.

The sNFW model is part of the general double-power law family investigated by [Zhao \(1996\)](#) and subsequently studied in detail by [An & Zhao \(2013\)](#), namely

$$\rho(r) = \frac{C}{r^\gamma(1+r^{1/\alpha})^{(\beta-\gamma)\alpha}},\quad (4)$$

★ E-mail: ejl44,nwe,jls@cam.ac.uk

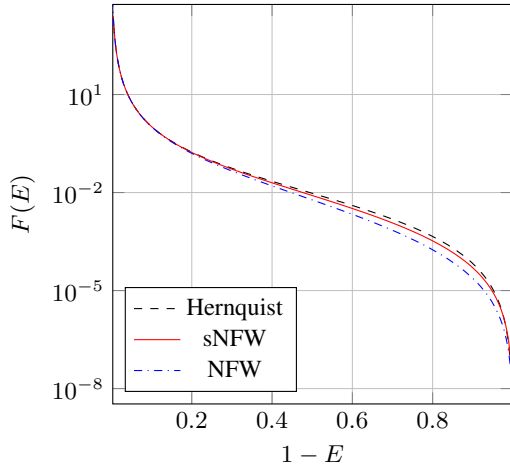


**Figure 1.** The isotropic DFs  $F(E)$  of the sNFW model (red) compared to the DFs of the Hernquist model (black) and NFW model (blue). The three models have the same central value of the potential and the same halo scalelength  $r_s$ .

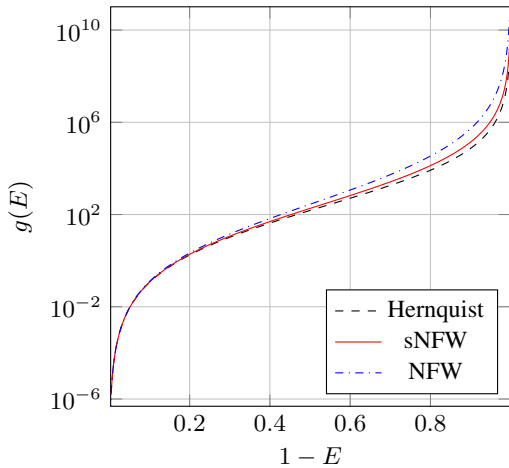


**Figure 2.** The density of states  $g(E)$  of the super-NFW model (red) compared to the Hernquist (black) and NFW (blue) models.

where  $C$  is a normalisation constant. In Zhao's notation, the sNFW model has  $(\alpha, \beta, \gamma) = (1, 3.5, 1)$ . Zhao was the first to note that the potential is simple. The sNFW model is also the  $b = 7/2$  member of the generalized NFW family

$$\rho(r) = \frac{C}{r(1+r)^{b-1}}, \quad (5)$$

studied in [Evans & An \(2006\)](#), who give asymptotic results for the dynamical quantities for the whole family. In general, however, biorthogonal basis sets for these entire families of models are not known, meaning that it is hard to build axisymmetric or triaxial analogues. This, however, is not the case for the sNFW model, as we show in our accompanying Paper II.

## 2 THE MODEL

### 2.1 Isotropic distribution functions

Let us use units in which  $G = a = 1$  and  $M = 2$ , so that the central value of the sNFW potential is  $\psi_{\text{sNFW}}(0) = 1$ . The enclosed mass

is

$$M(r) = 2 - \frac{2+3r}{(1+r)^{3/2}}, \quad (6)$$

so that the half-mass radius is  $r_{1/2} = 7.29086$ .

The potential  $\psi(r)$  can be inverted simply by setting  $x = \sqrt{1+r}$  and solving the resulting quadratic in  $x$ ; the form of  $r(\psi)$  is then

$$r(\psi) = \frac{4 - \psi - \sqrt{\psi(8+\psi)}}{2\psi}, \quad (7)$$

so that the density  $\rho$  can be expressed as

$$\rho(\psi) = \frac{3\psi \left(4 - \psi + \sqrt{\psi(8+\psi)}\right) \left(\psi + \sqrt{\psi(8+\psi)}\right)^5}{2^{16}\pi(1-\psi)}. \quad (8)$$

The isotropic distribution function (DF) is then given by [Edgington \(1916\)](#) as

$$F(E) = \frac{1}{\sqrt{8}\pi^2} \frac{d}{dE} \left[ \int_0^E \frac{d\rho}{d\psi} \frac{d\psi}{\sqrt{E-\psi}} \right], \quad (9)$$

This can be evaluated exactly as

$$F(E) = \frac{3}{7 \cdot 2^{10}\pi^3(8+E)(1-E)^2} \left[ 252 \frac{8+E}{\sqrt{2(1-E)}} \arcsin \sqrt{E} \right. \\ \left. + P_1(E)\sqrt{\frac{E}{2}} + P_2(E)E\left(-\frac{E}{8}\right) + P_3(E)K\left(-\frac{E}{8}\right) \right. \\ \left. + 189(8+E)\Pi\left(E, -\frac{E}{8}\right) \right], \quad (10)$$

where  $E$ ,  $K$  and  $\Pi$  are complete elliptic integrals and the  $P_i$  are the polynomials given in Appendix A. This is more complicated than the isotropic DF of the Hernquist Model, but simpler than the isotropic DF of the NFW model, which was first numerically constructed ([Widrow 2000](#); [Łokas & Mamon 2001](#)) and then analytically derived by [Evans & An \(2006\)](#).

In Fig. 1, we show the isotropic DF of this model against that of the Hernquist and NFW models. To compare all three models, we use the *halo scalelength*  $r_s$ , which is defined as the radius at which the logarithmic slope of the density attains the isothermal value, that is

$$\left. \frac{d \log \rho}{d \log r} \right|_{r=r_s} = -2. \quad (11)$$

For the Hernquist model we find  $r_s = b/2$ ; for sNFW  $r_s = 2a/3$ , and for NFW the initial choice of  $r_s$  already satisfies this property. As the form of the cusp is the same at small radii ( $\rho \sim 1/r$ ), so the DFs of all three models diverge like  $(1-E)^{-5/2}$  as  $E \rightarrow 1$ . However, for stars close to the binding energy ( $E \rightarrow 0$ ), the Hernquist DF behaves like  $E^{5/2}$ , the sNFW like  $E^2$  and the NFW like  $E^{3/2}$ . The density of states is

$$g(E) = (4\pi)^2 \int_0^{r_E} r^2 \sqrt{2(E-\psi)} dr \quad (12)$$

where  $r_E$  is the maximum radius of orbit with energy  $E$  ([Binney & Tremaine 1987](#)). After some calculation, we obtain

$$g(E) = \frac{4\sqrt{2}\pi^2}{3E^2} \left\{ 12 \arccos\left(\sqrt{E}\right) \frac{1+E}{\sqrt{E}} + 12(1-E)^{3/2}(2E+3) \right. \\ \left. + \sqrt{8+E} \left[ (2E^2+7E-16) E(\phi, \kappa^2) + E(1-2E) F(\phi, \kappa^2) \right] \right\}, \quad (14)$$

where  $F$  and  $E$  are incomplete elliptic integrals<sup>1</sup>, with argument

<sup>1</sup> Note that we use the *Mathematica* convention for the arguments of the elliptic functions, so that  $E(\phi, m) = \int_0^\phi d\theta \sqrt{1-m \sin^2 \theta}$ .

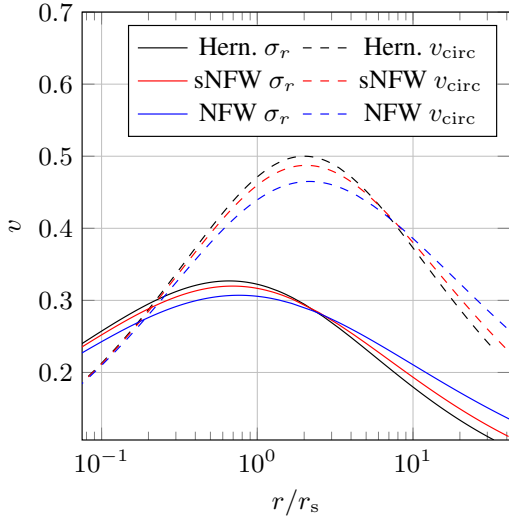


**Figure 3.** The velocity dispersion (full) and rotation curve (dotted) of the sNFW model (red) compared to the Hernquist (black) and NFW (blue) models plotted against radius (in units of  $r_s$ ). Note the peaks of the rotation curve and velocity dispersion of the models are comparable, but the decline for the Hernquist model takes place more quickly than for the sNFW and NFW models.

$\phi \equiv \arctan \sqrt{(1-E)/E}$  and modulus  $\kappa^2 \equiv 8/(8+E)$ . The density of states for the sNFW model is compared to that of the Hernquist and NFW models in Fig. 2.

The isotropic velocity dispersion is

$$\begin{aligned} \langle v_r^2 \rangle &= \frac{1}{6r(1+r)} \left[ 6 - 9r - 176r^2 - 406r^3 - 350r^4 - 105r^5 \right. \\ &\quad \left. - \sqrt{1+r} \left( 6 - 12r - 88r^2 - 120r^3 - 48r^4 \right) \right. \\ &\quad \left. + 3r^2(1+r)^{7/2} \left( 35 \operatorname{arccosh} \sqrt{r} - 16 \log \left( 1 + \frac{1}{r} \right) \right) \right]. \end{aligned} \quad (15)$$

The circular velocity curve (or rotation curve) is

$$v_{\text{circ}}^2 = \frac{2(1+r)^{3/2} - 3r - 2}{r(1+r)^{3/2}}. \quad (16)$$

In Fig. 3, the velocity dispersion profile and the circular velocity curve are shown for this model, as well as for the Hernquist and NFW models. Both the velocity dispersion and the rotation curve of the sNFW model have the desirable feature that they fall off much more slowly than for the Hernquist model. This is useful in modelling elliptical galaxies. For example, Gerhard et al. (2001) found that the circular velocity profiles of giant ellipticals are flat to within 10 to 20 per cent between  $0.2R_e$  to at least  $2R_e$ , independent of luminosity.

## 2.2 Anisotropic distribution functions

Analyses of kinematic data suggest that most elliptical galaxies are close to isotropic (Gerhard et al. 2001). Anisotropy is usually parametrized via

$$\beta = 1 - \frac{\langle v_\theta^2 \rangle + \langle v_\phi^2 \rangle}{2\langle v_r^2 \rangle}, \quad (17)$$

where angled brackets denote averages over the DF. Gerhard et al. (2001) find that  $-0.5 \lesssim \beta \lesssim 0.5$  in their study of giant ellipticals. Mild radial anisotropy is most common, though some tangen-

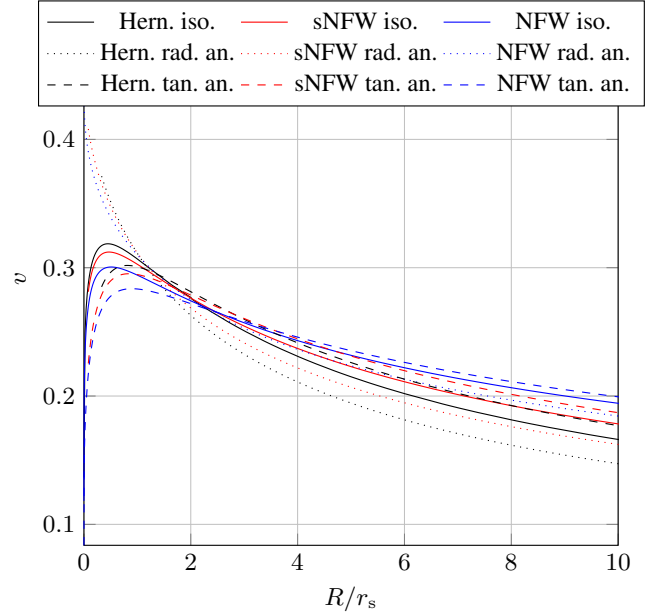


**Figure 4.** The line of sight velocity dispersions for the sNFW, Hernquist and NFW models plotted against projected distance (in units of  $r_s$ ). Full lines are the isotropic model, dotted radially anisotropic ( $\beta = \frac{1}{2}$ ) and dashed tangentially anisotropic ( $\beta = -\frac{1}{2}$ ).

tial anisotropic elliptical galaxies are known. We now develop two models that bracket the range of relevant anisotropies.

The DF of a spherical system with constant anisotropy is

$$F(E, L) = L^{-2\beta} f_E(E). \quad (18)$$

The unknown function  $f_E(E)$  can be recovered from the integral inversion formula (see e.g., Wilkinson & Evans 1999; Evans & An 2006)

$$f_E(E) = \frac{2^\beta (2\pi)^{-3/2}}{\Gamma(1-\lambda)\Gamma(1-\beta)} \frac{d}{dE} \int_0^E \frac{d\psi}{(E-\psi)^\lambda} \frac{d^n h}{d\psi^n}, \quad (19)$$

where  $h = r^{2\beta} \rho$  is expressed as a function of  $\psi$ , and  $n = \lfloor (3/2 - \beta) \rfloor$  and  $\lambda = 3/2 - \beta - n$  are the integer floor and the fractional part of  $3/2 - \beta$ . This includes the Eddington (1916) formula for the isotropic DF as a special case ( $\beta = 0$ ).

For the radially anisotropic model when  $\beta = 1/2$ , the expression for the DF reduces to

$$F(E, L) = \frac{1}{2\pi^2} \frac{1}{L} \left. \frac{dh}{d\psi} \right|_{\psi=E} = \frac{f_E(E)}{L}, \quad (20)$$

which for our model becomes

$$f_E(E) = \frac{15 \left( E + \sqrt{E(E+8)} + 4 \right) \left( E + \sqrt{E(E+8)} \right)^4}{2^{13} \pi \sqrt{E(E+8)}}. \quad (21)$$

The radial velocity dispersion is

$$\begin{aligned} \langle v_r^2 \rangle &= \frac{1}{6r(r+1)} \left[ 12 \left( \sqrt{r+1} - 1 \right) + 10r^3 \left( -6r + 3\sqrt{r+1} - 20 \right) \right. \\ &\quad \left. + 75r^2 \sqrt{r+1} - 232r + 55\sqrt{r+1} - 104r \right. \\ &\quad \left. + 30r(r+1)^{7/2} \left( \log \left( \frac{r}{r+1} \right) + 2 \operatorname{arccsch} \sqrt{r} \right) \right]. \end{aligned} \quad (22)$$

The analogous radially anisotropic ( $\beta = 1/2$ ) DFs for the Hernquist model is very simple and was discovered by [Baes & Dejonghe \(2002\)](#) and [Evans & An \(2005\)](#).

For the tangentially anisotropic model when  $\beta = -1/2$ , the expression for the DF further reduces to

$$F(E, L) = \frac{L}{2\pi^2} \left. \frac{d^2 h}{d\psi^2} \right|_{\psi=E} = L f_E(E), \quad (23)$$

where

$$f_E(E) = \frac{3E^{3/2}(E + \sqrt{E(E+8)})^4(36 - 19E - 5E^2 + \sqrt{E(E+8)}(9 - 3E))}{2^{12}\pi^3\sqrt{E+8}(1-E)(E + \sqrt{E(8+E)} - 4)^2} \quad (24)$$

whilst the second moment is

$$\begin{aligned} \langle v_r^2 \rangle = & \frac{1}{12r(r+1)} \left[ -15r^3(r+1)^{7/2}(2\operatorname{arcsch}\sqrt{r} + 8\log\frac{r}{r+1}) \right. \\ & + 8(\sqrt{r+1}-1) + 5r^2(6\sqrt{r+1}-7) + 44r^3(5\sqrt{r+1}-12) \\ & \left. - 3r^4(406 - 100\sqrt{r+1}) - 5r^5(21r - 8\sqrt{r+1} + 70) \right]. \quad (25) \end{aligned}$$

Fig. 4 shows the line of sight velocity dispersions for the sNFW model for the three choices of anisotropy ( $\beta = \frac{1}{2}, 0$  and  $-\frac{1}{2}$ ). The equivalent results for the Hernquist and NFW models are also shown. As expected, radial anisotropy leads to an enhancement of the line of sight dispersion near the centre (where the dotted curves lie above the full curves). Tangential anisotropy causes the line of sight dispersions to be enhanced above the isotropic case in the outer parts (where the dashed curves lie above full curve). Note that the line of sight dispersion profiles of the sNFW model show a more gradual decline with distance than the Hernquist model. This is in good accord with the data on nearly round elliptical galaxies, which show slow declines out to  $\approx 2R_e$  ([Kronawitter et al. 2000](#)).

Overall, the sNFW model gives somewhat more complicated expressions for quantities (such as the DFs) than the Hernquist model. The pay-back is that the density profile falls off more slowly ( $\rho_{\text{sNFW}} \sim r^{-3.5}$ ) and so the rotation curve and velocity dispersion profiles are much flatter. This is much more like the observed behaviour of elliptical galaxies and dark matter haloes.

### 3 COMPARISONS

#### 3.1 Sersic and de Vaucouleurs Profile

Traditionally, the light profiles of elliptical galaxies and bulges have been fit by the [de Vaucouleurs \(1953\)](#) profile, which is

$$\log_{10} \left( \frac{\Sigma(R)}{\Sigma(R_e)} \right) = -3.331 \left[ \left( \frac{R}{R_e} \right)^{1/4} - 1 \right]. \quad (26)$$

Here,  $R_e$  is the effective radius, or the radius of the isophote that encloses half the luminosity. [Caon et al. \(1993\)](#) examined the photometric profiles of a large sample of elliptical galaxies and argued for use of the more general [Sersic \(1968\)](#) law

$$\log_{10} \left( \frac{\Sigma(R)}{\Sigma(R_e)} \right) \approx 0.8686(0.1635 - n) \left[ \left( \frac{R}{R_e} \right)^{1/n} - 1 \right], \quad (27)$$

where the Sersic index  $n$  satisfies  $2 \lesssim n \lesssim 10$ . The de Vaucouleurs profile is the case  $n = 4$ , whilst  $n = 1$  corresponds to an exponential. The photometric profiles of bulges were studied by [Andredakis](#)

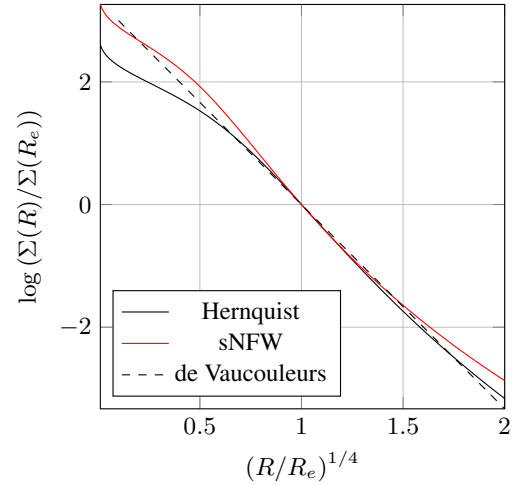


**Figure 5.** The surface density of the sNFW model (red), the Hernquist model (black) and the de Vaucouleurs profile (dashed).

[et al. \(1995\)](#), who found that bulges of S0s are well-fit by a de Vaucouleurs profile, whilst bulges of late-type spirals are better fit by an exponential.

To compare the sNFW model against these photometric laws, we must first compute its projected density. This is

$$\Sigma(R) = \frac{(R+1)(R+3) \operatorname{K}\left(\frac{R-1}{2R}\right) - 8R \operatorname{E}\left(\frac{R-1}{2R}\right)}{2^{3/2}\pi\sqrt{R}(R^2-1)^2}. \quad (28)$$

The half-light or effective radius is  $R_e = 1.81527$ . Assuming a constant mass-to-light ratio, Fig. 5 shows the surface brightness of the de Vaucouleurs profile, together with the Hernquist and sNFW models between 0.1 and  $2R_e$ . The sNFW model is a better global fit than the Hernquist model to the de Vaucouleurs profile. Beyond  $\approx 5R_e$ , however, the sNFW surface density falls off rather more slowly than both the Hernquist and de Vaucouleurs profiles.

More formally, we can fit the projected densities of both the Hernquist and sNFW models between 0.1 and  $2R_e$  to the Sersic profiles. The Hernquist model gives  $n = 3.388$  and the sNFW  $n = 4.200$ . Given the range of properties of elliptical galaxies and bulges, both profiles are useful. The Hernquist model is a better match to  $n \approx 3$  Sersic profiles, whilst the sNFW is a better match to  $n \approx 4$  (de Vaucouleurs profile).

#### 3.2 Numerical halo fitting

Dark matter halos are often parametrised in terms of their virial mass  $M_v$ , virial radius  $r_v$  and concentration  $c$  ([Diemer & Kravtsov 2015](#)). The virial mass is the mass contained within a spherical shell of radius  $r_v$ , that is  $M_v = M(r_v)$ . Once a particular model is chosen to fit the halo, the length scale is parametrised using the concentration parameter  $c = r_v/r_s$ , where  $r_s$  is the halo scalelength as defined in Eq. (11). For the NFW model, in the notation of equation (2), we have

$$\rho_{\text{NFW}} = \frac{M_v}{4\pi} \left( \log(1 + c_{\text{NFW}}) - \frac{c_{\text{NFW}}}{1 + c_{\text{NFW}}} \right)^{-1} \frac{1}{r(r + r_v/c_{\text{NFW}})^2}. \quad (29)$$

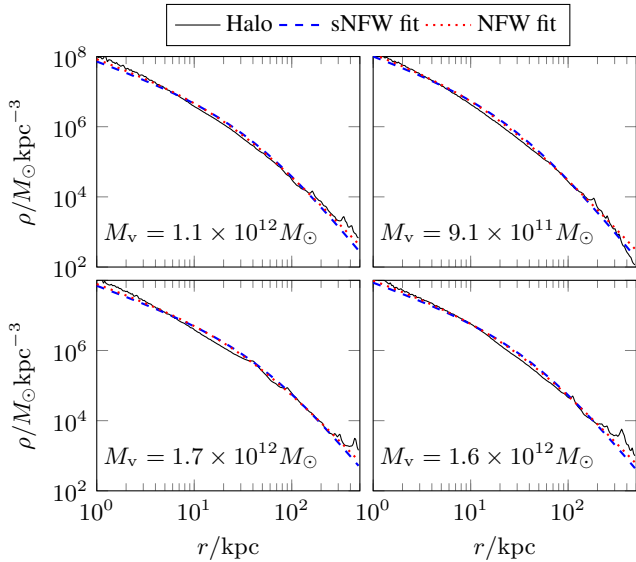


**Figure 6.** Fits of the sNFW and NFW models to the radial density profile of four dark matter haloes extracted from a cosmological  $N$ -body simulation. The numerical halo data is binned logarithmically, and the virial mass of each halo is inlaid.

The analogous definition for the sNFW model is

$$\rho_{\text{sNFW}} = \frac{3^{3/2} M_v}{8\pi} \left( 1 - \frac{1 + c_{\text{sNFW}}}{(1 + 2c_{\text{sNFW}}/3)^{3/2}} \right)^{-1} \frac{(r_v/c_{\text{sNFW}})^{1/2}}{r (2r + 3r_v/c_{\text{sNFW}})^{5/2}}. \quad (30)$$

We have fitted both the NFW and sNFW model to ten numerically-constructed dark matter haloes extracted from cosmological simulations (for more details on their provenance, see Paper II). Four of these fits are shown in Fig. 6, and the relation between the derived concentration parameters for the two models, along with a best fit line, is shown in Fig. 7. We notice that the sNFW model does at least as good a job as the NFW profile in fitting the shapes of these ten haloes. The concentration  $c_{\text{sNFW}}$  of the best-fit sNFW model is related to that of the best-fit NFW model via

$$c_{\text{sNFW}} = 1.36 + 0.76c_{\text{NFW}} \quad (31)$$

This gives an easy way to transform the mass-concentration relations for NFW models, given for example in equations (8) and (9) of Dutton & Macciò (2014), to provide a cosmologically-inspired sequence of sNFW dark haloes.

## 4 CONCLUSIONS

We have introduced the super-NFW (sNFW) model. This is a potential-density pair useful for representing spherical bulges, elliptical galaxies and dark haloes. The radial force component is very simple, namely

$$F_r = \nabla\psi = \frac{\sqrt{a}GM}{r^2\sqrt{a+r}} + \frac{\sqrt{a}GM}{2r(a+r)^{3/2}} - \frac{GM}{r^2} \quad (32)$$

This should make the model useful for  $N$ -body work.

The density of the sNFW model falls like  $\rho_{\text{sNFW}} \sim r^{-1}$  near the centre, and like  $\rho_{\text{sNFW}} \sim r^{-3.5}$  on the outskirts. This gives it two important advantages over competitors like the Hernquist

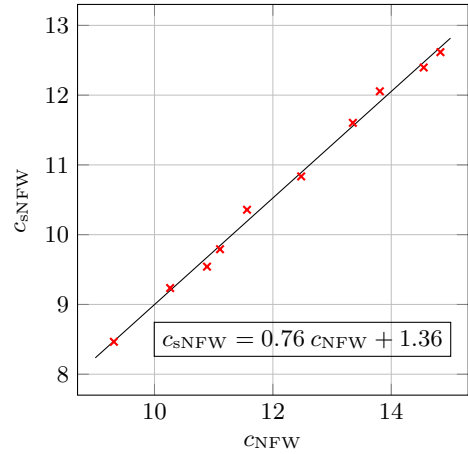


**Figure 7.** Concentrations for 10 numerical haloes as fitted by the sNFW and NFW models. The line of best fit is shown.

model: First, it is a better match to the de Vaucouleurs profile in the inner parts, so it is useful for modelling the light profiles of elliptical galaxies and bulges. Its density falls off somewhat more slowly than the Hernquist model ( $\rho_{\text{H}} \sim r^{-4}$ ), which makes it a better match to the line of sight velocity dispersion profiles of ellipticals at large radii. Secondly, the asymptotic density fall-off is closer to the density profile of numerically-constructed haloes, which approximately follow the Navarro-Frenk-White (NFW) form and have  $\rho_{\text{NFW}} \sim r^{-3}$  at large radii. The advantage of using a sNFW model rather than an NFW model is that we have provided a suite of DFs (isotropic, radially and tangentially anisotropic) for the sNFW model, whereas the DFs of the NFW model are not elementary (Evans & An 2006).

There are of course many other models with central density cusps like  $\rho \sim r^{-1}$  and with asymptotic decays between  $\rho \sim r^{-3}$  and  $\rho \sim r^{-4}$  (e.g., An & Evans 2006) or halo models with finite mass (e.g., Navarro et al. 2004; Zhao & Silk 2005). In particular, An & Zhao (2013) provide a compendium of properties of spherical double-power-law models, some of which can also provide equally good matches to the density profiles of dark haloes. However, these models do not readily generalise to arbitrary distorted geometries. We show in our companion Paper II that the sNFW model has another remarkable property. It can be used to form a new bi-orthonormal basis function expansion in a manner analogous to that discovered by Hernquist & Ostriker (1992) for the Hernquist model itself. Amongst other advantages, this means that the model can be easily extended to flattened, triaxial and lopsided geometries.

The intrinsic properties of our model (such as the DFs and velocity dispersions) are more complicated than the Hernquist model, but less complicated than the NFW model. We conclude that the sNFW model provides an excellent trade-off between simplicity and realism in modelling dark haloes and elliptical galaxies.

## ACKNOWLEDGEMENTS

EJL and JLS acknowledge financial support from the Science and Technology Facilities Council. We thank Denis Erkal for providing us with a suite of numerically constructed cosmological haloes, as well as the referees for constructive comments.

**REFERENCES**

- An, J. H., & Evans, N. W. 2006, *AJ*, 131, 782  
 An, J. H., Zhao, H. 2013, *MNRAS*, 428, 2805  
 Andredakis, Y. C., Peletier, R. F., & Balcells, M. 1995, *MNRAS*, 275, 874  
 Baes, M., Dejonghe, H. 2002, *A&A*, 393, 485  
 Binney, J., Tremaine, S., 2008, *Galactic Dynamics*, Princeton University Press, Princeton  
 Caon, N., Capaccioli, M., & D’Onofrio, M. 1993, *MNRAS*, 265, 1013  
 Cappellari, M. 2016, *ARA&A*, 54, 597  
 de Vaucouleurs, G. 1953, *MNRAS*, 113, 134  
 Diemer, B. & Kravtsov, A. V. 2015, *ApJ*, 799, 108  
 Diemer, B., Mansfield, P., Kravtsov, A. V., & More, S. 2017, *ApJ*, 843, 140  
 Dutton, A. A., & Macciò, A. V. 2014, *MNRAS*, 441, 3359  
 Eddington, A.S. 1916, *MNRAS*, 76, 572  
 Evans, N.W., An, J.H. 2005, *MNRAS*, 360, 492  
 Evans, N.W., An, J.H. 2006, *Phys. Rev. D.*, 73, 023524  
 Gerhard, O., Kronawitter, A., Saglia, R. P., & Bender, R. 2001, *AJ*, 121, 1936  
 Hernquist, L. 1990, *ApJ*, 356, 359  
 Hernquist, L., Ostriker, J. P. 1992, *ApJ*, 386, 375  
 Kronawitter, A., Saglia, R. P., Gerhard, O., & Bender, R. 2000, *A&AS*, 144, 53  
 Lilley E., Sanders J.L., Evans N.W., Erkal D. 2017, *MNRAS*, submitted (Paper II)  
 Lokas, E. L., & Mamon, G. A. 2001, *MNRAS*, 321, 155  
 Navarro, J. F., Frenk, C. S., White, S. D. M. 1997, *ApJ*, 490, 493  
 Navarro, J. F., Hayashi, E., Power, C., et al. 2004, *MNRAS*, 349, 1039  
 Sersic, J. L. 1968, Cordoba, Argentina: Observatorio Astronomico, 1968,  
 Widrow, L. M. 2000, *ApJS*, 131, 39  
 Wilkinson, M.I., Evans, N.W. 1999, *MNRAS*, 310, 645  
 Zhao, H. 1996, *MNRAS*, 278, 488  
 Zhao, H., & Silk, J. 2005, *Physical Review Letters*, 95, 011301

**APPENDIX A: AUXILIARY FUNCTIONS**

Here, we record some auxiliary functions used in the DF of the super-NFW model. They are

$$\begin{aligned}
 P_1(E) &= -4(32E^6 + 416E^5 + 1200E^4 - 920E^3 - 2198E^2 + 399E + 504) \\
 P_2(E) &= -8(32E^6 + 352E^5 + 656E^4 - 1176E^3 - 586E^2 + 173E + 360) \\
 P_3(E) &= (E + 8)(128E^5 + 512E^4 - 576E^3 - 480E^2 + 56E + 171)
 \end{aligned}$$

This paper has been typeset from a  $\text{\TeX}/\text{\LaTeX}$  file prepared by the author.